Biophys Rep 2025, 11(X):1–10
https://doi.org/10.52601/bpr.2025.250031 https://cstr.cn/32402.14.bpr.2025.250031
Biophysics Reports

RESEARCH ARTICLE

[^{64}Cu]Cu-NOTA-Ivonescimab: a novel PET tracer for imaging VEGF expression in colorectal carcinoma

Wenpeng Huang[1,2#], Yongshun Liu[3#], Ruobing Li[4#], Yihan Yang[1], Jessica C. Hsu[2], Molly C. DeLuca[2], Jonathan W. Engle[2], Yuchun Wei[5] ✉, Lei Kang[1] ✉, Liming Li[6] ✉, Weibo Cai[2] ✉

[1] Department of Nuclear Medicine, Peking University First Hospital, Beijing 100034, China
[2] Departments of Radiology and Medical Physics, University of Wisconsin – Madison, Madison, WI 53705, USA
[3] Department of Medical Imaging, Peking University First Hospital, Beijing 100034, China
[4] University of Wisconsin – Madison, Madison, WI 53705, USA
[5] Department of Radiation Oncology, Shandong Cancer Hospital and Institute, Shandong First Medical University and Shandong Academy of Medical Sciences, Jinan 250117, China
[6] Department of Radiology, The First Affiliated Hospital of Zhengzhou University, Zhengzhou 450052, China

Received: 23 May 2025 / Accepted: 23 July 2025

Abstract Colorectal cancer (CRC) has high rates of recurrence and metastasis, underscoring the need for improved diagnostic imaging methods to support accurate disease monitoring and inform treatment decisions. In this study, we present [^{64}Cu]Cu-NOTA-Ivonescimab, a novel ImmunoPET tracer that specifically targets vascular endothelial growth factor-A (VEGF-A), which is upregulated in CRC. Ivonescimab was conjugated to a NOTA chelator and radiolabeled with copper-64, achieving over 99% radiochemical purity and demonstrating robust *in vitro* stability. *In vivo* PET imaging of HCT-116 CRC xenograft models showed specific, time-dependent tumor uptake of [^{64}Cu]Cu-NOTA-Ivonescimab, peaking at 13.73 ± 0.95 %ID/g at 48 h post-injection. This was significantly higher than in the blocking group (5.20 ± 0.10 %ID/g, P = 0.00011). Furthermore, Ivonescimab conjugated with the near-infrared dye IRDye 800CW allowed complementary optical imaging, displaying significantly higher fluorescence intensity in tumors (25.49 ± 8.69 × 10^8 p/(s·cm^2·sr)) compared to blocking controls (4.66 ± 0.95 × 10^8 p/(s·cm^2·sr), P = 0.0145) at 48 h post-injection. Together, these findings establish [^{64}Cu]Cu-NOTA-Ivonescimab as a promising imaging agent that offers precise, non-invasive quantification of VEGF expression, with potential to enhance diagnostic accuracy and guide therapy in CRC.

Keywords ImmunoPET, Cu-64, VEGF, Radioactive tracer, Positron emission tomography, Colorectal cancer

INTRODUCTION

Colorectal cancer (CRC) is the third most prevalent cancer worldwide and ranks second in cancer-related deaths. Despite advances in chemotherapy, CRC remains associated with high recurrence and metastasis rates (Zhou *et al*. 2023). Anti-angiogenic therapy has emerged as a key treatment strategy, as tumor angiogenesis drives cancer progression and metastasis (Yan *et al*. 2024). Vascular endothelial growth factor-A (VEGF-A) serves as a predominant regulator of

Electronic supplementary material The online version of this article contains supplementary material, which is available to authorized users.

[#] Wenpeng Huang, Yongshun Liu and Ruobing Li contributed equally to this work.

✉ Correspondence: yuchunwei0000@foxmail.com (Y. Wei), kanglei@bjmu.edu.cn (L. Kang), perfect1989a@163.com (L. Li), wcai@uwhealth.org (W. Cai)

angiogenesis across various malignancies and pathological conditions. Consequently, monoclonal antibodies targeting VEGF, such as bevacizumab and aflibercept, have shown good prospects in suppressing angiogenesis by neutralizing VEGF in the tumor microenvironment (García-Varela *et al*. 2024).

Preclinical studies have indicated that combining anti-VEGF therapies with immune checkpoint inhibitors, such as anti-PD-(L)1 antibodies, can produce synergistic antitumor effects by engaging dual mechanisms of action (Manegold *et al*. 2017; Zhao *et al*. 2022). Ivonescimab, a novel bispecific antibody that targets both PD-1 and VEGF-A, was developed to enhance therapeutic precision while minimizing systemic toxicity in tumors co-expressing these targets (Frentzas *et al*. 2024). Approved in China in May 2024 for patients with EGFR-mutant NSCLC following resistance to EGFR-TKIs, Ivonescimab represents a significant advance in immunotherapy (Dhillon 2024; Frentzas *et al*. 2024; Zhang *et al*. 2025). However, there is still a lack of effective biomarkers to predict treatment response or monitor resistance to Ivonescimab therapy.

Although VEGF is a well-validated therapeutic target, clinical imaging methods for assessing VEGF expression remain limited. Conventional imaging modalities, such as contrast-enhanced CT or MRI, primarily assess morphological changes or vascular permeability rather than molecular VEGF expression. As a result, they often lack the sensitivity and specificity needed for accurately quantifying VEGF activity, particularly for monitoring therapeutic response or predicting treatment outcomes.

ImmunoPET, a highly sensitive molecular imaging technique, combines antibodies or antibody fragments with positron- or gamma-emitting radionuclides to provide real-time, *in vivo* visualization of specific molecular targets (Huang *et al*. 2025a, d). This approach has shown strong potential for optimizing therapeutic strategies in CRC (Li *et al*. 2023; Touchefeu *et al*. 2021).

In this study, we employed ImmunoPET imaging to assess VEGF expression in CRC models with [^{64}Cu]Cu-NOTA-Ivonescimab. We also conjugated Ivonescimab to the near-infrared fluorescence (NIRF) dye IRDye 800CW, allowing complementary optical imaging of tumors without ionizing radiation. The [^{64}Cu]Cu-NOTA-Ivonescimab tracer offers non-invasive, whole-body imaging and provides detailed insight into dynamic VEGF expression and tumor targeting over time. This imaging capability empowers clinicians to precisely evaluate the biodistribution, tumor-specific uptake, and retention kinetics of Ivonescimab in real time. Ultimately, quantitative ImmunoPET imaging with Ivonescimab may serve as a valuable companion diagnostic, helping to predict therapeutic efficacy, refine dosing regimens, and identify patients most likely to benefit from VEGF-targeted therapies.

RESULTS

Radiosynthesis of [^{64}Cu]Cu-NOTA-Ivonescimab

The conjugation of NOTA to Ivonescimab and subsequent labeling with ^{64}Cu is illustrated in Fig. 1. The labeling yield prior to purification was 84.48 ± 2.54% (n = 5) (supplementary Fig. S1A). Following purification using PD-10 columns, the radiochemical purity of the final product exceeded 99% (n = 5) (supplementary Fig. S1B). *In vitro* stability assessments demonstrated that [^{64}Cu]Cu-NOTA-Ivonescimab maintained a radiochemical purity exceeding 95% after 48 h of incubation in 0.01 mol/L PBS and 5% human serum albumin, confirming the probe's excellent stability (supplementary Figs. S1C–S1D).

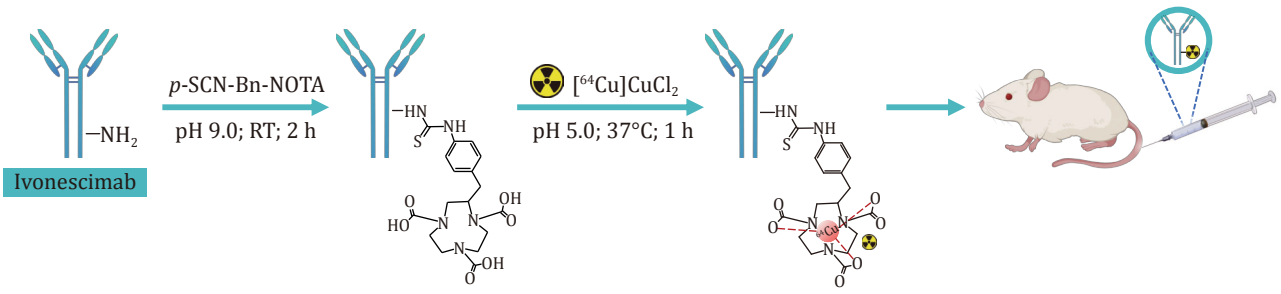

Fig. 1 Synthetic scheme of [^{64}Cu]Cu-NOTA-Ivonescimab. Ivonescimab was first functionalized with *p*-SCN-Bn-NOTA at pH 9.0 for 2 h at room temperature, followed by radiolabeling with [^{64}Cu]$CuCl_2$ at pH 5.0 and 37°C for 1.0 h. [^{64}Cu]Cu-NOTA-Ivonescimab was purified to obtain the final product for subsequent applications

ImmunoPET imaging and quantitative analysis

Colorectal carcinoma models were constructed using HCT-116 cell lines. Maximum intensity projection (MIP) images were acquired between 1 to 48 h post-injection of [^{64}Cu]Cu-NOTA-Ivonescimab (Fig. 2). The tracer clearly delineated tumor morphology as early as 12 h post-injection, with tumor uptake progressively increasing and reaching a peak at 48 h post-injection. In contrast, minimal tumor uptake was observed in the blocking groups, indicating target-specific binding.

Quantitative ROI analysis revealed time-dependent uptake of [^{64}Cu]Cu-NOTA-Ivonescimab in HCT-116 tumors. At 12 h post-injection, tumor uptake was 7.80 ± 0.85 %ID/g, rising to a maximum of 13.73 ± 0.95 %ID/g at the final time point (48 h post-injection) before sacrifice (Fig. 3A). Blocking with excess unlabeled Ivonescimab significantly reduced tracer accumulation in tumors, with uptake decreasing to 5.20 ± 0.10 %ID/g (P = 0.00011). Uptake in non-target organs, including the heart, liver, spleen, and kidneys, gradually decreased over time.

At 48 h post-injection, [^{64}Cu]Cu-NOTA-Ivonescimab demonstrated significantly higher target-to-non-target (T/NT) ratios (Fig. 3B). The tumor-to-heart (blood) ratio in HCT-116 tumors without blockade reached 1.32 ± 0.13, which was significantly reduced to 0.40 ± 0.03 in the blocking group (P = 0.0003). Similarly, the tumor-to-muscle ratio was 15.62 ± 0.98 in the non-blocked group compared to 6.33 ± 0.65 with blocking (P = 0.0002), further supporting the specificity of tumor targeting by the radiotracer.

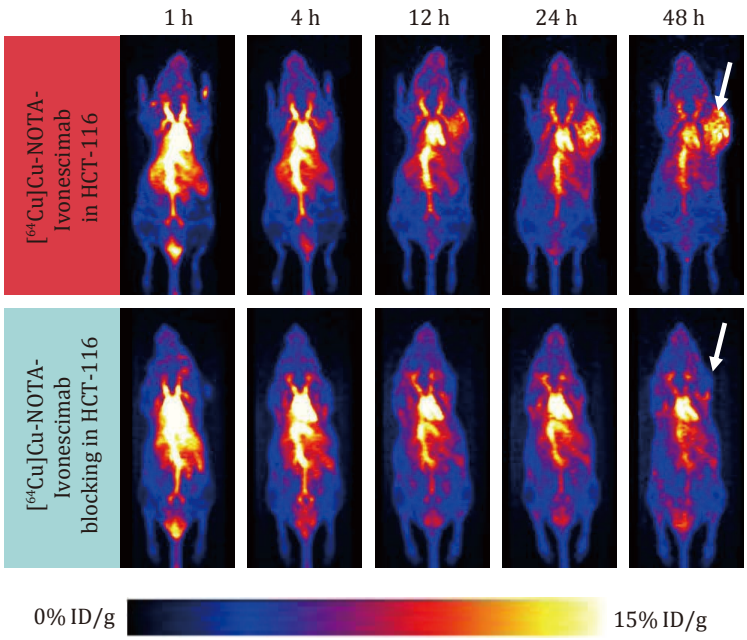

Fig. 2 Longitudinal PET imaging of HCT-116 tumor-bearing mice after injection of [^{64}Cu]Cu-NOTA-Ivonescimab with or without blocking. Maximum intensity projection (MIP) PET images were acquired at 1, 4, 12, 24, and 48 h post-injection. The top row shows prominent and time-dependent tumor accumulation of [^{64}Cu]Cu-NOTA-Ivonescimab in HCT-116 xenografts (white arrows indicate tumor site). Tumor uptake became clearly distinguishable by 12 h post-injection and peaked at 48 h. In contrast, the blocking group (bottom row), which received excess unlabeled Ivonescimab, showed markedly reduced tumor signals, confirming the tracer's target specificity. The color scale represents %ID/g (0–15)

Biodistribution results

At 48 hours post-injection, *ex vivo* biodistribution analysis (Fig. 4) showed high tumor uptake in the HCT-116 group treated with [^{64}Cu]Cu-NOTA-Ivonescimab (13.67 ± 0.95 %ID/g). In contrast, tumor uptake in the blocking group was significantly decreased (4.07 ± 0.25 %ID/g, P = 0.00007).

NIRF imaging and ROI-based analysis

After administration of 150 μg of IRDye 800CW-Ivonescimab, tumors were conspicuous from 6 to 168 h post-injection. Fluorescence intensity in the IRDye 800CW-Ivonescimab group was significantly higher than in the blocking group, indicating that co-injection of excess unlabeled Ivonescimab effectively inhibited

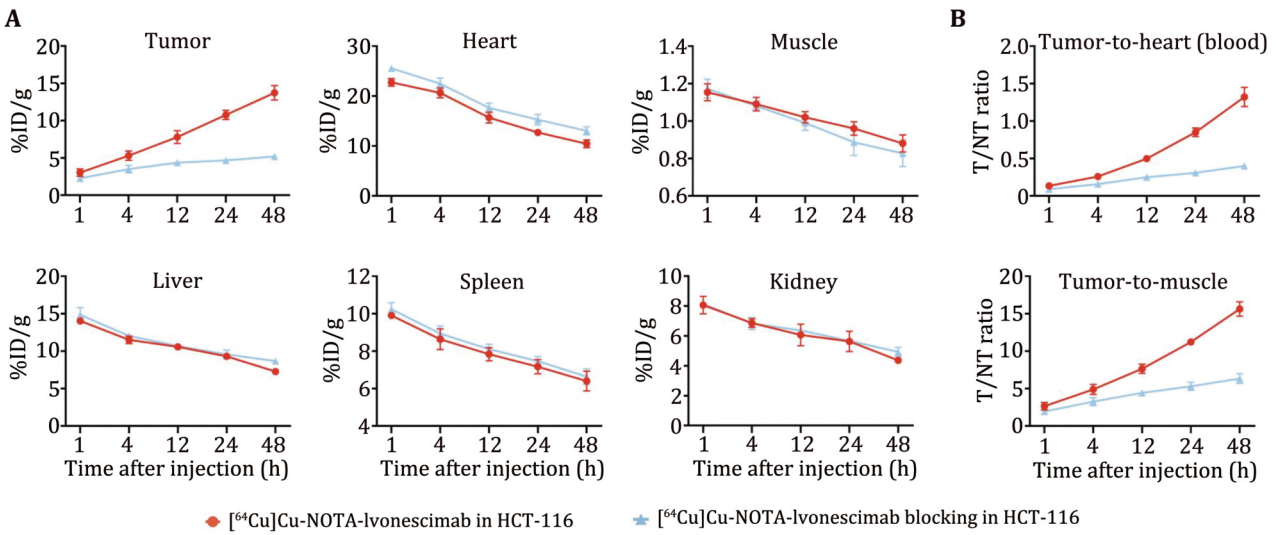

Fig. 3 Quantitative biodistribution and target-to-non-target (T/NT) analysis of [^{64}Cu]Cu-NOTA-Ivonescimab in HCT-116 tumor-bearing mice with or without blocking. **A** Quantitative biodistribution data (%ID/g) of the radiotracer in the tumor and major organs over time. **B** Tumor-to-heart and tumor-to-muscle ratios over time as determined by region-of-interest image analyses. Data are presented as mean ± SD (n = 3)

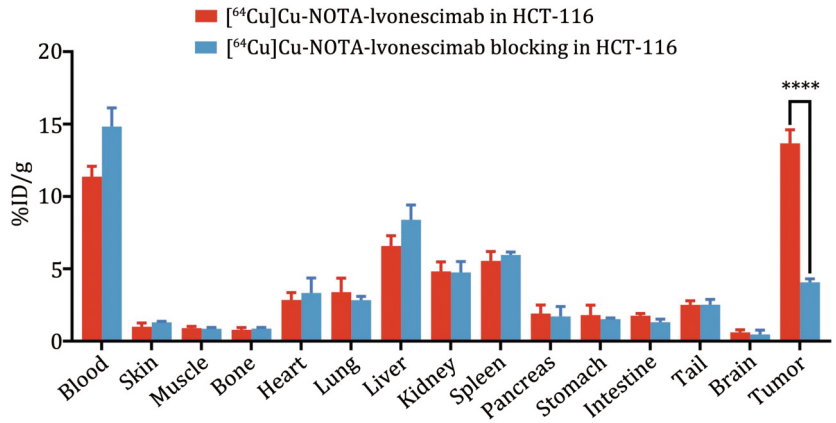

Fig. 4 *Ex vivo* biodistribution of [^{64}Cu]Cu-NOTA-Ivonescimab in HCT-116 tumor-bearing mice at 48 h post-injection. Quantitative biodistribution analysis revealed high tumor uptake of [^{64}Cu]Cu-NOTA-Ivonescimab in the non-blocked group (13.67 ± 0.95 %ID/g), while significantly reduced tumor accumulation was observed in the blocking group (4.07 ± 0.25 %ID/g, P = 0.00007). Uptake in other major organs (*e.g.*, liver, kidney, spleen) showed no significant differences between the groups, indicating specific tumor targeting. Data are presented as mean ± SD (n = 3 per group). Statistical analysis was performed using the unpaired two-tailed Student's t-test; ****P < 0.0001

binding of the fluorescently-labeled antibody to HCT-116 tumors (Fig. 5A). This observation was further supported by *ex vivo* organ fluorescence imaging. Notably high fluorescence was observed in the liver and kidneys, which are likely sites of Ivonescimab metabolism and excretion (Fig. 5B).

Semi-quantitative ROI analysis showed that tumor uptake in the IRDye 800CW-Ivonescimab group was significantly higher than in the blocking group (Fig. 6A). The specific binding of IRDye 800CW-Ivonescimab to HCT-116 tumors (25.49 ± 8.69 × 10^8 p/(s·cm^2·sr) at 48 h) was significantly greater than the blocking group (4.66 ± 0.95 × 10^8 p/(s·cm^2·sr) at 48 h, P = 0.0145).

Ex vivo organ fluorescence quantification of harvested organs corroborated these findings (Fig. 6B). Significant tumor accumulation was observed in the

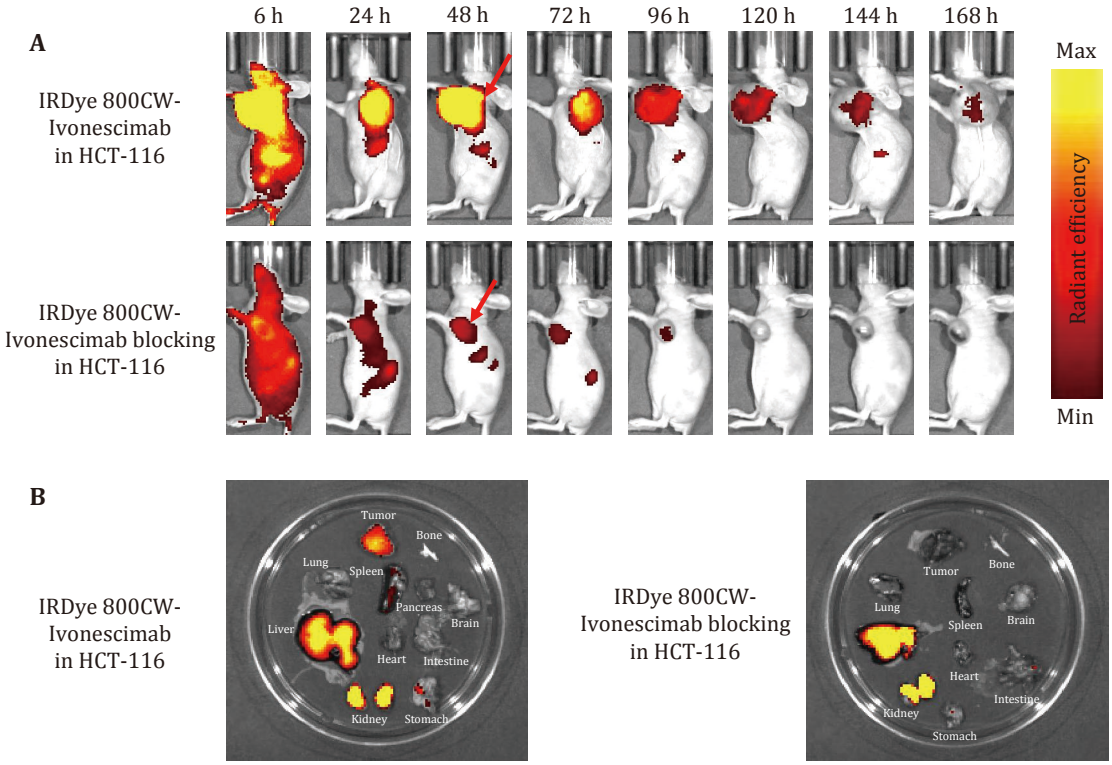

Fig. 5 *In vivo* and *ex vivo* fluorescence imaging of IRDye 800CW-labeled Ivonescimab in HCT-116 tumor-bearing mice. **A** Serial fluorescence images from 6 to 168 h post-injection show strong, tumor-specific accumulation of IRDye 800CW-Ivonescimab in the non-blocked group, with clear tumor visualization persisting for up to one week. In contrast, fluorescence signals were markedly reduced in the blocking group, indicating successful competition by excess unlabeled Ivonescimab and confirming target-specific binding. **B** *Ex vivo* imaging at 168 h post-injection revealed prominent fluorescence in tumors of the non-blocked group, with much lower signal intensity in the blocking group. High fluorescence was observed in the liver and kidneys of both groups, likely reflecting sites of antibody metabolism and excretion. Organs were arranged in the dish as labeled for comparison. The color bar represents radiant efficiency from minimum to maximum

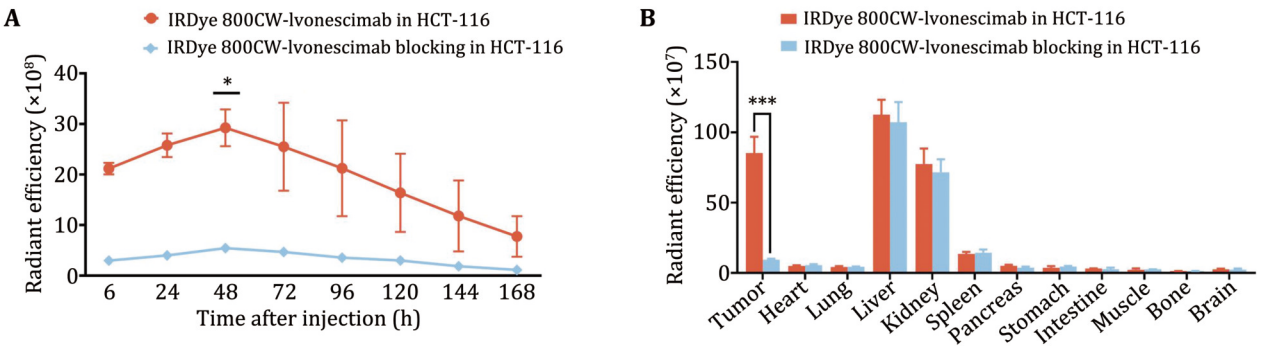

Fig. 6 Quantitative analysis of *in vivo* and *ex vivo* fluorescence imaging of IRDye 800CW-Ivonescimab in HCT-116 tumor-bearing mice. **A** Time-dependent, semi-quantitative ROI analysis demonstrated significantly higher tumor uptake in the IRDye 800CW-Ivonescimab group compared to the blocking group. At 48 h post-injection, tumor fluorescence reached 25.49 ± 8.69 × 10^8 p/(s·cm^2·sr) in the non-blocked group versus 4.66 ± 0.95 × 10^8 p/(s·cm^2·sr) in the blocking group (P = 0.0145), confirming specific binding. **B** *Ex vivo* fluorescence quantification of major organs at 168 h post-injection revealed markedly elevated tumor signal in the IRDye 800CW-Ivonescimab group (85.28 ± 11.38 × 10^7 p/(s·cm^2·sr)) compared to the blocking group (9.45 ± 0.70 × 10^7 p/(s·cm^2·sr), $^{**}P$ = 0.0003). High fluorescence in the liver and kidneys was observed in both groups, consistent with antibody metabolism and excretion. Data are presented as mean ± SD (n = 3 per group); statistical significance was determined by unpaired two-tailed t-test ($^*P < 0.05$, $^{**}P < 0.001$)

IRDye 800CW-Ivonescimab group compared to the blocking group (85.28 ± 11.38 × 10^7 p/(s·cm^2·sr) *vs.* 9.45 ± 0.70 × 10^7 p/(s·cm^2·sr) at 168 h for the HCT-116 model, P = 0.0003). From these results, fluorescently-labeled Ivonescimab effectively targeted VEGF-expressing tumors *in vivo*, demonstrating its potential as a diagnostic imaging agent for CRC detection.

H&E staining

Histological examination showed normal tissue architecture across various major organs, with no signs of inflammation or pathological damage following radiotracer administration (Fig. 7).

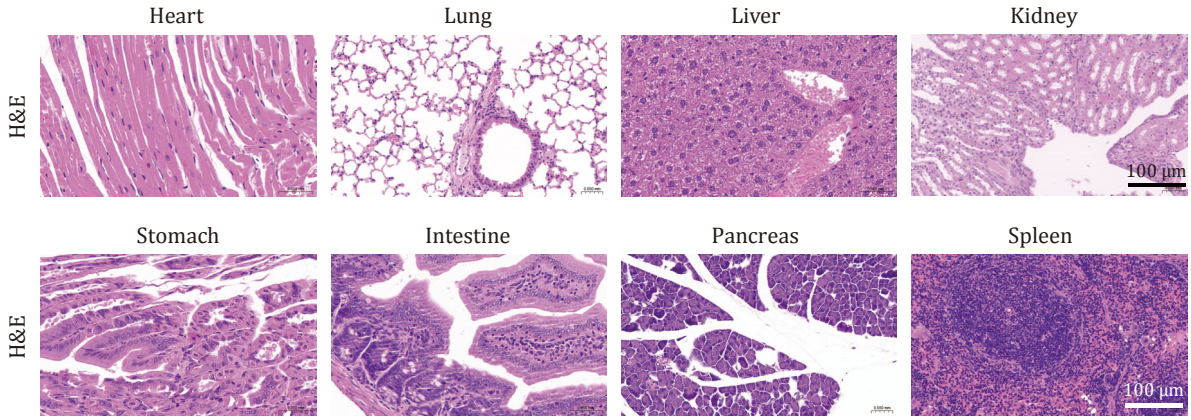

Fig. 7 Hematoxylin and eosin (H&E) staining of major organs following radiotracer administration. Histology of the heart, lung, liver, kidney, stomach, intestine, pancreas, and spleen revealed well-preserved tissue architecture with no signs of inflammation, necrosis, or other pathological changes. Scale bar: 100 μm

Immunofluorescence staining

Immunofluorescence staining was performed to assess vascularization (CD31) and VEGF expression in the tumor and surrounding normal tissues. Tumors derived from HCT-116 xenografts showed abundant CD31-positive vasculature along with strong VEGF expression (Fig. 8).

In non-tumor tissues, CD31 staining revealed well-defined vascular structures throughout, while VEGF expression was negligible compared to that in tumor tissue.

Extrapolation of radiation dosimetry to humans

Dosimetry was assessed using OLINDA/EXM software (Stabin *et al.* 2005). Human radiation doses were estimated from %ID/g values obtained via PET imaging in BALB/c mice, assuming comparable biodistribution in humans. Absorbed doses were calculated using OLINDA output data in combination with tissue weighting factors from ICRP Publication 103 (2007). The estimated effective dose for an adult female was 0.036 mSv/MBq (Table 1), aligning with established safety standards in nuclear medicine research.

DISCUSSION

Noninvasive ImmunoPET is an advanced molecular imaging approach that offers high specificity, affinity, and sensitivity through antibody-based targeting (Huang *et al.* 2025c, e). This technique enables real-time, dynamic visualization of molecular targets, such as VEGF, supporting precise monitoring of tumor biology and therapeutic response (Huang *et al.* 2025b).

In May 2024, Ivonescimab became the first bispecific antibody approved by China's National Medical Products Administration (NMPA) for clinical use. It was approved in combination with chemotherapy for patients with locally advanced or metastatic EGFR-mutant non-squamous NSCLC who had progressed following EGFR-TKI therapy. Ivonescimab uniquely targets both PD-1 and VEGF-A, representing a significant advance in the field of cancer immunotherapy (Crescioli *et al.* 2025; Sankar and Reckamp 2025). In our study, we employed [^{64}Cu]Cu-NOTA-Ivonescimab for ImmunoPET imaging in preclinical CRC models, achieving high-resolution and quantitative delineation of VEGF expression. To further enhance spatial resolution and extend imaging capability, we integrated near-infrared fluorescence imaging using IRDye 800CW-conjugated Ivonescimab. This dual-modality

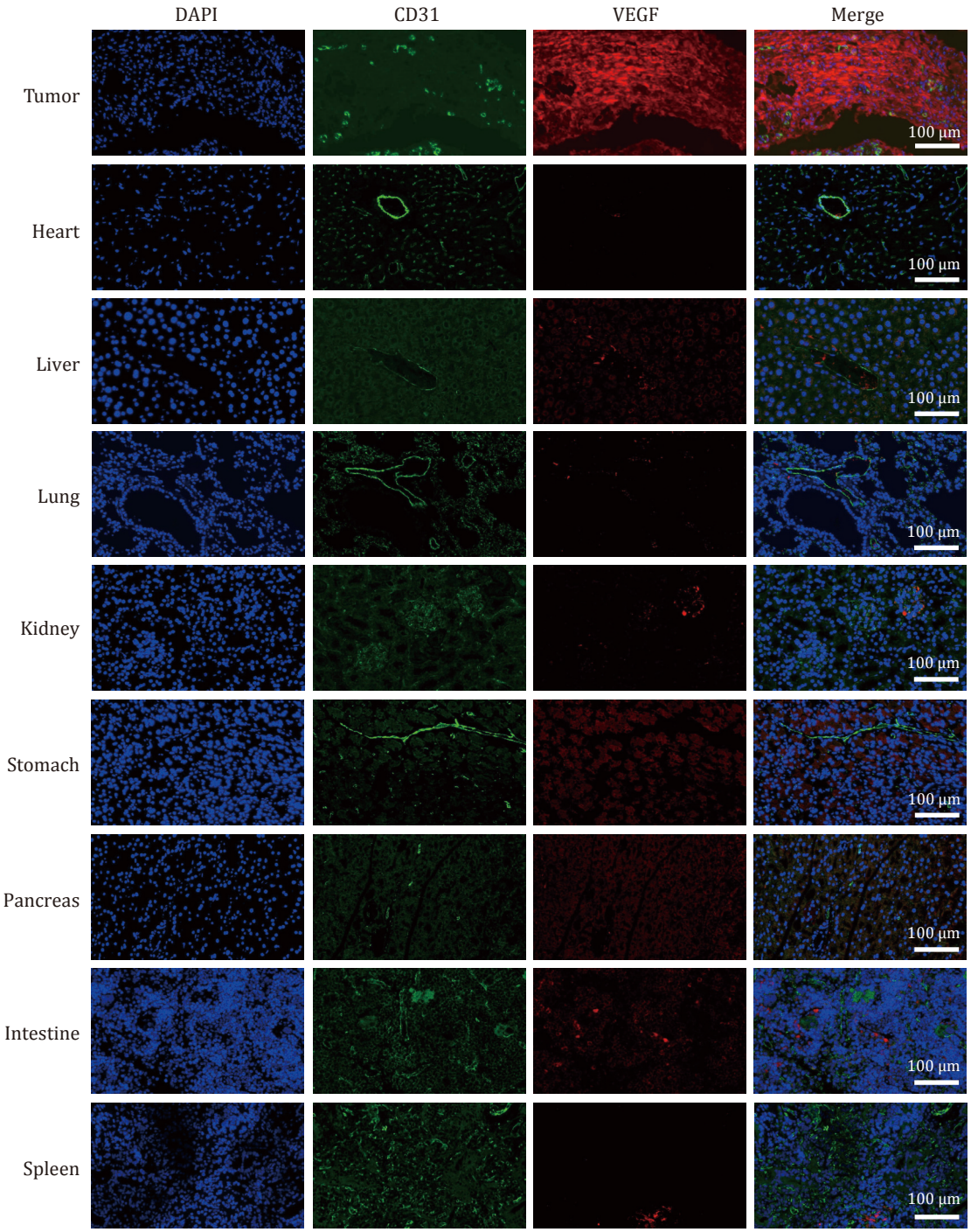

Fig. 8 Immunofluorescence staining of VEGF expression and vascularization (CD31) in tumor and major organs. Representative images of tumor and normal tissues stained with DAPI (blue), CD31 (green), and VEGF (red) demonstrate prominent vascularization and high VEGF expression in HCT-116 tumors. In contrast, normal organs — including heart, liver, lung, kidney, stomach, pancreas, intestine, and spleen — exhibited well-defined CD31-positive vascular structures but minimal VEGF expression. These results confirm the tumor-specific overexpression of VEGF and support the rationale for VEGF-targeted imaging and therapeutic strategies. Scale bar: 100 μm

strategy provides complementary visualization, especially beneficial for fluorescence-guided surgical interventions.

Prior studies have confirmed the feasibility and utility of VEGF-targeted ImmunoPET in preclinical oncology (Chen *et al.* 2024; Meyer *et al.* 2016). Meyer *et*

Table 1 Human organ radiation dosimetry estimation of [^{64}Cu]Cu-NOTA-Ivonescimab

Target organ	mSv/MBq
Adrenals	3.19×10^{-4}
Brain	8.94×10^{-5}
Breasts	3.39×10^{-3}
Esophagus	1.32×10^{-3}
Gallbladder wall	3.04×10^{-4}
Left colon	1.71×10^{-3}
Small intestine	3.40×10^{-4}
Stomach wall	4.49×10^{-3}
Right colon	1.63×10^{-3}
Rectum	7.80×10^{-4}
Heart wall	1.03×10^{-3}
Kidneys	3.19×10^{-4}
Liver	1.44×10^{-3}
Lungs	6.56×10^{-3}
Ovaries	1.36×10^{-3}
Pancreas	2.29×10^{-4}
Salivary glands	2.87×10^{-4}
Red marrow	6.77×10^{-3}
Osteogenic cells	3.84×10^{-4}
Spleen	3.05×10^{-4}
Thymus	3.27×10^{-4}
Thyroid	1.22×10^{-3}
Urinary bladder wall	1.20×10^{-3}
Uterus	1.56×10^{-4}
Effective dose	3.60×10^{-2}

al. (Meyer *et al*. 2016) pioneered two ^{89}Zr-labeled tracers, scVR1/Zr and scVR2/Zr, based on single-chain VEGF-A (scVEGF) variants with selective binding to VEGFR-1 and VEGFR-2, respectively. These innovative tracers demonstrated rapid tumor uptake and increasing tumor-to-blood ratios over time in orthotopic 4T1luc breast tumor-bearing BALB/c mouse models. Competitive inhibition experiments using an excess of unlabeled proteins demonstrated that over 80% of tumor uptake was receptor-mediated. Immunohistochemical analyses further differentiated receptor localization, revealing that VEGFR-1 was predominantly expressed on stromal and tumor cells, whereas VEGFR-2 was primarily found on CD31-positive endothelial cells, corroborating PET imaging data. Compared to scVR1/Zr and scVR2/Zr, the tracer [^{64}Cu]Cu-NOTA-Ivonescimab described in our study offers practical advantages by utilizing the clinically approved Ivonescimab antibody, thus streamlining clinical translation and broadening its theranostic potential.

In a recent preclinical study, Chen *et al*. (Chen *et al*. 2024) introduced a dual-modality theranostic strategy using aflibercept (Abe), a high-affinity decoy receptor that targets both VEGF and PlGF. Abe was labeled with ^{89}Zr for PET imaging and lutetium-177 for targeted radiotherapy in renal cancer models. In Renca tumor-bearing mice, the tracer [^{89}Zr]Zr-Abe exhibited significant and specific tumor uptake, with peak tumor-to-blood and tumor-to-muscle ratios reaching 2.17 ± 0.44 and 11.75 ± 3.59, respectively, at five days post-injection. Blocking studies confirmed target specificity, showing markedly reduced tracer uptake. These findings were further validated by complementary fluorescence imaging using Cy5.5-conjugated Abe, which showed highly selective tumor accumulation. Treatment with [^{177}Lu]Lu-Abe substantially suppressed tumor growth, with standardized tumor volumes reaching only 207.6 ± 49.5% by day 14, compared to 1064.3 ± 706.0% in the PBS control group ($P < 0.05$). These compelling results underscore the therapeutic benefit and clinical utility of VEGF-targeted theranostics.

In our work, Ivonescimab was directly radiolabeled to produce [^{64}Cu]Cu-NOTA-Ivonescimab, a radiotracer with high radiochemical purity, excellent *in vitro* stability, and VEGF-specific targeting in preclinical CRC models. Moreover, biodistribution studies and Immuno-PET imaging indicated notable hepatic uptake across all experimental groups, suggesting that liver metabolism and systemic circulation impact the tracer's pharmacokinetics. The gradual decline in hepatic signal over time aligns well with the known clearance profile of monoclonal antibodies cleared through hepatic pathways. Notably, [^{64}Cu]Cu-NOTA-Ivonescimab enables non-invasive, whole-body evaluation of VEGF expression, offering a major advantage over traditional biopsies and serum biomarkers, which often fail to capture the full extent and spatial heterogeneity of tumor burden.

Our findings present valuable insights into the pharmacokinetics and *in vivo* biodistribution of Ivonescimab, advancing our understanding of its translational relevance for VEGF-targeted therapies. Conjugation of Ivonescimab to IRDye 800CW allowed for extended fluorescence imaging, enabling detailed characterization of biodistribution over time and helping to determine the optimal therapeutic windows. Our dual-modality approach combines the deep-tissue, quantitative imaging capability of [^{64}Cu]Cu-NOTA-Ivonescimab with the real-time, high-resolution visualization provided by IRDye 800CW. Together, these complementary strengths offer a clinically relevant strategy that supports comprehensive cancer care, including diagnosis, treatment monitoring, and fluorescence-guided surgery.

PET imaging offers high sensitivity, deep tissue penetration, and accurate whole-body quantification of tracer distribution. NIRF imaging provides real-time, high-resolution visualization of superficial lesions, making it especially valuable for fluorescence-guided surgery. In contrast to previously reported VEGF-targeted tracers, our approach uses a single, clinically validated bispecific antibody scaffold to support both imaging modalities. This integration simplifies clinical translation and expands the potential for broader diagnostic and theranostic applications.

Nonetheless, this study has several limitations. The relatively small sample size in each experimental group warrants further validation in larger cohorts to confirm reproducibility and robustness. In more complex tumor models featuring tumor-infiltrating lymphocytes (TILs) and PD-1 expression, signal interpretation may be more challenging. Future work will focus on engineering smaller Ivonescimab fragments, such as $F(ab')_2$ (~110 kDa) or Fab (~55 kDa), to improve pharmacokinetics while maintaining high specificity and binding affinity.

CONCLUSION

In summary, this study demonstrates the successful conjugation of Ivonescimab to the NOTA chelator and subsequent radiolabeling with copper-64. Our approach produces [^{64}Cu]Cu-NOTA-Ivonescimab, a highly stable and pure tracer suitable for ImmunoPET imaging in preclinical colorectal cancer models. Our results underscore the strong potential of [^{64}Cu]Cu-NOTA-Ivonescimab as a versatile imaging agent for precise diagnosis, treatment monitoring, and therapeutic guidance in VEGF-expressing malignancies.

EXPERIMENTAL PROCEDURES

Materials and methods

A comprehensive evaluation of [^{64}Cu]Cu-NOTA-Ivonescimab was performed using various analytical methods. Athymic Nude-Foxn1nu mice (Envigo) bearing HCT-116 tumors were injected with [^{64}Cu]Cu-NOTA-Ivonescimab (7.4–11.1 MBq/100 μL), followed by PET imaging at 1, 4, 12, 24, and 48 h post-injection. *Ex vivo* biodistribution studies were conducted after each PET scan. To assess fluorescence-guided surgical potential, IRDye 800CW-labeled Ivonescimab was administered to HCT-116 tumor-bearing mice, with *in vivo* and *ex vivo* fluorescence imaging performed over a 7-d period. Blocking studies and quantitative fluorescence analysis were conducted to validate target specificity. Detailed experimental protocols and reagent information are available in the supplementary information.

RESOURCE AVAILABILITY

Lead contact

Further information and requests for resources should be directed to the lead contact, Weibo Cai (wcai@uwhealth.org).

Materials availability

This study did not generate novel unique materials.

Data and code availability

All data needed to evaluate the conclusions of the study are presented in the paper and the supplementary information.

Acknowledgements We are grateful for financial support from the University of Wisconsin – Madison and the National Institutes of Health (P30 CA014520), the National Natural Science Foundation of China (82472018, 82171970), Beijing Nova Program (20240484725), Beijing Municipal Science & Technology Commission (Z221100007422027), National Key Research and Development Program of China (2024YFE0113500), National High Level Hospital Clinical Research Funding (Interdisciplinary Research Project of Peking University First Hospital, 2023IR17, 2024IR07; Scientific and Technological Achievements Transformation Incubation Guidance Fund Project of Peking University First Hospital, 2024CX18), the Scientific and technological project in Henan Province (242102311026), The Key Research Project in Henan Universities (23A320059).

Author contributions W. H., L. K., and W. C.: Conceptualization, Project administration. W. H., Y. L., R. L., Y. Y.: Data curation, Formal analysis. W. H., L. L., Y. W.: Investigation, Methodology. M. D., J. E.: Resources. W. H.: Writing – original draft. J. H.: Writing – review & editing. L. L., L. K., W. C.: Funding acquisition, Supervision, Writing – review & editing.

Compliance with Ethical Standards

Conflict of interest Weibo Cai declares conflict of interest with the following corporations: Portrai, Inc., rTR Technovation Corporation, Four Health Global Pharmaceuticals Inc. All other authors declare no conflict of interest.

Human and animal rights and informed consent This article does not contain any studies with humans performed by any of the authors. All institutional and national guidelines for the care and use of laboratory animals were followed. The study was

approved by the Institutional Animal Care and Use Committee at the University of Wisconsin-Madison (#M005630), and the Animal Committee of Peking University First Hospital (No. J2023059).

References

Chen Z, Yang Q, Song LL, Qiu YK, Wang TY, Wu ST, Huang WP, Sun XY, Wang AX, Kang L (2024) Enhanced theranostic efficacy of ^{89}Zr and ^{177}Lu-labeled aflibercept in renal cancer: a viable option for clinical practice. Mol Pharm 21(5): 2544–2554

Clark ME, Larsson C, Gentner NE, Pentreath R, Chairman LH, Alexakhin RM, Loy J, Strand P, Bréchignac F, Pröhl G, Tsela AK, Carroll SA, Robinson CA, Woodhead D, Fujimoto K, Shpyth AA, Xuan Y (2008) Preface, executive summary and glossary. Ann ICRP 38: 11–17

Crescioli S, Kaplon H, Wang L, Visweswaraiah J, Kapoor V, Reichert JM (2025) Antibodies to watch in 2025. mAbs 17(1): 2443538. https://doi.org/10.1080/19420862.2024.2443538

Dhillon S (2024) Ivonescimab: first approval. Drugs 84(9): 1135–1142

Frentzas S, Austria Mislang AR, Lemech C, Nagrial A, Underhill C, Wang WJ, Wang ZM, Li BY, Xia Y, Coward JIG (2024) Phase 1a dose escalation study of ivonescimab (AK112/SMT112), an anti-PD-1/VEGF-A bispecific antibody, in patients with advanced solid tumors. J Immunother Cancer 12(4): e008037. https://doi.org/10.1136/jitc-2023-008037

García-Varela L, Codesido J, Perez-Pedrosa A, Muñoz-González M, Ramos-Docampo E, Rey-Bretal D, García-Otero X, Gómez-Lado N, Turrero A, Beiroa D, Rodríguez-Perez AI, Vidal A, Fernández-Ferreiro A, Pubul V, Aguiar P (2024) Biodistribution and pharmacokinetics of [^{89}Zr]-anti-VEGF mAbs using PET in glioblastoma rat models. Int J Pharm 652: 123795. https://doi.org/10.1016/j.ijpharm.2024.123795

Huang WP, Li LM, Liang YT, Yang Q, Mixdorf JC, Engle JW, Fan Y, Kang L, Cai WB (2025a) ImmunoPET imaging of Nectin4 expression in gastric and bladder cancer using [^{64}Cu]Cu-NOTA-Padcev. Mol Pharm 22(6): 3468–3478

Huang WP, Li LM, Zhou YH, Yang Q, Mixdorf JC, Barnhart TE, Hsu JC, Saladin RJ, Liu CH, Rosenkrans ZT, Engle JW, Gao JB, Kang L, Cai WB (2025b) Preclinical evaluation of zirconium-89 labeled anti-Trop2 antibody-drug conjugate (Trodelvy) for imaging in gastric cancer and triple-negative breast cancer. Eur J Nucl Med Mol Imaging 52(7): 2369–2383

Huang WP, Wang TY, Chao FF, Yang Q, Mixdorf JC, Li LM, Engle JW, Fan Y, Kang L, Cai WB (2025c) ImmunoPET imaging of Trop2 expression in bladder cancer using [^{64}Cu]Cu-NOTA-Trodelvy. Mol Pharm 22(4): 2266–2275

Huang WP, Wang TY, Qiu YK, Li CZ, Chen B, Song LL, Yang Q, Sun XY, Jia B, Kang L (2025d) CD38-specific immunoPET imaging for multiple myeloma diagnosis and therapeutic monitoring: preclinical and first-in-human studies. Eur J Nucl Med Mol Imaging 52(5): 1791–1804

Huang WP, Zhang YW, Xiao XY, Yang Q, Mixdorf JC, Sun XY, Engle JW, Fan Y, Li LM, Kang L, Cai WB (2025e) ImmunoPET imaging of Trop2 expression in triple-negative breast cancer using [^{64}Cu]Cu-NOTA-Trodelvy-F(ab')$_2$. Eur J Nucl Med Mol Imaging 52(9): 3223–3237

Li LQ, Lin XF, Wang L, Ma XP, Zeng ZQ, Liu FT, Jia B, Zhu H, Wu AW, Yang Z (2023) Immuno-PET of colorectal cancer with a CEA-targeted [68 Ga]Ga-nanobody: from bench to bedside. Eur J Nucl Med Mol Imaging 50(12): 3735–3749

Manegold C, Dingemans A-MC, Gray JE, Nakagawa K, Nicolson M, Peters S, Reck M, Wu Y-L, Brustugun OT, Crinò L, Felip E, Fennell D, Garrido P, Huber RM, Marabelle A, Moniuszko M, Mornex F, Novello S, Papotti M, Pérol M, Smit EF, Syrigos K, van Meerbeeck JP, van Zandwijk N, Chih-Hsin Yang J, Zhou CC, Vokes E (2017) The potential of combined immunotherapy and antiangiogenesis for the synergistic treatment of advanced NSCLC. J Thorac Oncol 12(2): 194–207

Meyer J-P, Edwards KJ, Kozlowski P, Backer MV, Backer JM, Lewis JS (2016) Selective imaging of VEGFR-1 and VEGFR-2 using ^{89}Zr-labeled single-chain VEGF mutants. J Nucl Med 57(11): 1811–1816

Sankar K, Reckamp KL (2025) Ivonescimab in advanced NSCLC: is progression-free survival enough, or are overall survival data also needed? Lancet 405(10481): 757–759. https://doi.org/10.1016/S0140-6736(25)00369-1

Stabin MG, Sparks RB, Crowe E (2005) OLINDA/EXM: the second-generation personal computer software for internal dose assessment in nuclear medicine. J Nucl Med 46(6): 1023–1027

Touchefeu Y, Bailly C, Frampas E, Eugène T, Rousseau C, Bourgeois M, Bossard C, Faivre-Chauvet A, Rauscher A, Masson D, David A, Cerato E, Carlier T, Sharkey RM, Goldenberg DM, Barbet J, Kraeber-Bodere F, Bodet-Milin C (2021) Promising clinical performance of pretargeted immuno-PET with anti-CEA bispecific antibody and gallium-68-labelled IMP-288 peptide for imaging colorectal cancer metastases: a pilot study. Eur J Nucl Med Mol Imaging 48(3): 874–882

Yan M, Yang RH, Li Q, Wang CJ, Chen JL, Wu ZY, Li H, Fan J (2024) Anti-angiogenic and antitumor effects of anlotinib combined with bevacizumab for colorectal cancer. Transl Oncol 41: 101887. https://doi.org/10.1016/j.tranon.2024.101887

Zhang Y, Liu XY, Ren SX (2025) Ivonescimab in non-small cell lung cancer: harmonizing immunotherapy and anti-angiogenesis. Expert Opin Biol Ther 25(5): 499–505

Zhao YS, Guo SP, Deng J, Shen J, Du FK, Wu X, Chen Y, Li MX, Chen MJ, Li XB, Li WP, Gu L, Sun YH, Wen QL, Li J, Xiao ZG (2022) VEGF/VEGFR-targeted therapy and immunotherapy in non-small cell lung cancer: targeting the tumor microenvironment. Int J Biol Sci 18(9): 3845–3858

Zhou SZ, Sun DZ, Mao WJ, Liu Y, Cen W, Ye LC, Liang F, Xu JM, Shi HC, Ji Y, Wang LS, Chang WJ (2023) Deep radiomics-based fusion model for prediction of bevacizumab treatment response and outcome in patients with colorectal cancer liver metastases: a multicentre cohort study. eClinicalMedicine 65: 102271. https://doi.org/10.1016/j.eclinm.2023.102271

